Elastic and inelastic quasiparticle tunneling between anisotropic superconductors

Yung-mau Nie and L. Coffey
Illinois Institute of Technology, Chicago, Illinois 60616
(Received 26 May 1998; revised manuscript received 7 October 1998)

Numerical results are presented for quasiparticle tunneling across a superconductor-insulator-superconductor (SIS) tunnel junction due to elastic and inelastic tunneling, with the latter mediated by spin fluctuations and phonons. SIS tunnel junctions with $d_{x^2-y^2}$, extended $s+d_{x^2-y^2}$, and extended $s+id_{x^2-y^2}$ superconducting order-parameter symmetries are investigated. The dependence of the tunneling conductance (dI/dV) on temperature, directional tunneling matrix element, and a tight-binding band structure appropriate for high-temperature superconductors is studied. The results are compared with recent point-contact tunneling and scanning tunneling microscope measurements of SIS tunneling dI/dV curves for optimal and overdoped $Bi_2Sr_2CaCu_2O_8$. [S0163-1829(99)05817-8]

I. INTRODUCTION

Recent point-contact tunneling (PCT) and scanning tunneling microscope (STM) experiments[1,2] have revealed interesting behavior in the superconductor-insulator-superconductor (SIS) tunneling conductance curves (dI/dV) of the high-temperature superconductor (HTSC) $Bi_2Sr_2CaCu_2O_8$ (Bi2212). The peak, at a bias voltage which corresponds to $2\Delta(T)$, where $\Delta(T)$ is identified as the superconducting gap, is accompanied by an unusual high bias voltage behavior which displays a dip at approximately $3\Delta(T)$ on a low, flat background. Furthermore, when the tunneling conductance for optimally doped and overdoped Bi2212 is measured in these experiments, the measured gap $\Delta(T)$ decreases while the dip feature in the measured dI/dV maintains its position at $3\Delta(T)$ and appears to become shallower in the more overdoped samples.

The aim of this paper is to interpret this latest data using a combination of elastic and spin-fluctuation-mediated inelastic directional tunneling between anisotropic superconductors. The present calculations of the quasiparticle tunneling dI/dV for an SIS junction are an extension of our previous work[3] on the voltage and temperature dependence of the supercurrent across similar types of model junctions as are examined in the present work.

Early results[4,5] on HTSC SIS junctions demonstrated dip features in dI/dV curves similar to those observed in Refs. 1, 2 in a selection of HTSC with gap values and critical temperature varying over a large range, demonstrating that the dip is an intrinsic feature of the HTSC state. However, the most widely cited experimental studies of HTSC SIS junctions have focused on measurements of the phase of the superconducting gap and on measurements of the temperature and magnetic field dependence of the Josephson current[6,7] in $YBa_2Cu_3O_7$. These experiments have provided strong evidence for a $d_{x^2-y^2}$ symmetry superconducting gap in $YBa_2Cu_3O_7$ (YBCO). More recent experiments on Pb-YBCO SIS junctions indicate the possibility of a mixed *s*-wave and *d*-wave gap in YBCO.[8]

Theoretical work on HTSC junctions includes proposals to explain the dip feature in experimental HTSC dI/dV curves in terms of a one to three quasiparticle decay mode[9,10] or by using a combination of elastic and inelastic tunneling.[11,12] The dip feature is most prominent in SIS dI/dV curves but can also be observed in STM superconductor-insulator–normal-metal[13] and angle-resolved photoemission spectroscopy (ARPES) measurements on Bi2212.[14] The emergence of the dip feature below T_c and the observation that the position of the dip is always close to $3\Delta(T)$ in a range of SIS dI/dV curves suggests that the position of the dip feature is determined by the energy threshold at which quasiparticle emission of antiferromagnetic spin fluctuations (AFMSF's) occurs in HTSC. The position of the dip feature, which can be understood to be a consequence of the feedback of superconducting correlations into quasiparticle interactions below T_c, may also be evidence of an anisotropic superconducting state, such as the proposed $d_{x^2-y^2}$ state for the HTSC cuprates. The ideas of Refs. 9 and 12 are closely related but not identical viewpoints of the underlying physics producing the dip feature.

AFMSF's play an important role in HTSC (Ref. 15) and it is the aim of the present work to extend previous investigations[11,12] of how inelastic AFMSF emission processes by electrons at low temperature might provide an explanation for the dip and the type of background observed in some tunneling experiments at higher bias voltages. Previous work by one of the present authors[11,12] on inelastic, tunneling mediated by emission of spin fluctuations, proposed a possible explanation for the dip feature seen in HTSC dI/dV curves and ARPES originating from the development of a spin gap due to superconductivity in the AFM susceptibility. The quasiparticle spectral weight curves generated in this type of approach may explain recent angle-resolved photoemission spectroscopy (ARPES) results on Bi2212 where a large inelastic background, with a dip feature, is observed in the data.[14]

There also exists a large body of theoretical work on the role of quasiparticle scattering at interfaces in generating zero-energy peaks in the density of states, in suppressing a $d_{x^2-y^2}$ superconducting gap locally at an interface and in generating various mixed symmetry superconducting gaps such as the time-reversal symmetry breaking $s+id$ state.[16–20] The present work will focus on tunnel junctions in which the normal to the junction is along the crystalline *x*

axis and in which tunneling also occurs primarily along this direction. In this case, no zero-energy peaks are predicted in the density of states and so the effect of these can be ignored. The effect of a mixed symmetry extended $s+id$ state is investigated in the present work, however.

Another important feature of the present work is the incorporation of tunneling directionality into calculations of the dI/dV curves for quasiparticle tunneling in SIS junctions. The assumption of some degree of directional tunneling has been implicit in analyses of Pb-YBCO junction experiments[6] and YBCO rings on tricrystal substrates[7] which have been used to investigate the phase of the superconducting gap. Tunneling directionality, which is incorporated into calculations of the dI/dV via a momentum-dependent tunneling matrix element, is particularly important in studying the HTSC materials because of the anisotropy intrinsic to the electronic properties of the copper oxide planes of the HTSC coming from the shape of the Fermi surface, the Van Hove singularity associated with the $(\pi,0)$ Brillouin-zone (BZ) point, and the $d_{x^2-y^2}$ symmetry gap with its line of nodes along the BZ diagonal.

The remainder of this paper consists of Sec. II in which the theoretical formalism is presented and Sec. III in which numerical results are discussed. The quasiparticle tunneling curves (dI/dV) are calculated with a tight-binding band structure and various superconducting gaps including $d_{x^2-y^2}$, extended $s+id_{x^2-y^2}$, and extended $s+d_{x^2-y^2}$ symmetries. A tunneling matrix element is used in the calculations which selects out a line of k states in the BZ of the superconductors on either side of the junction along the x axis with the normal to the tunneling interface assumed to be along this same axis. A phenomenological spectral weight function for AFMSF's is used for the inelastic quasiparticle tunneling channel which incorporates the qualitative shape and superconducting feedback effect that were calculated microscopically in Ref. 12.

Finally, the contribution of phonon-mediated inelastic tunneling is investigated in the present work using a realistic phonon spectral weight $\alpha^2F(\omega)$ for the Bi2212 material.[21]

II. FORMALISM

The elastic and inelastic quasiparticle tunneling current can be expressed as[22,23]

$$I_{\rm qp}^{\rm el}(V,T)=4e/\hbar\int\frac{dE}{\pi}[f(E)-f(E+eV)]N(E)n(E+eV) \tag{1}$$

and

$$I_{\rm qp}^{\rm inel}(V,T)=4e/\hbar\int\frac{dE}{\pi}\int\frac{dE'}{\pi}[1-f(E)-f(eV-E)]\times[f(E')+n(E'-E+eV)]D(E'-E+eV)\times N(E)N(E'), \tag{2}$$

where $f(E)$ and $n(E)$are the Fermi-dirac and Bose-Einstein distribution functions. The spectral weight of spin fluctuations or phonons is incorporated through $D(E)$. The tunneling density of states of quasiparticles, $N(E)$, is defined as

$$N(E)=\sum_{\mathbf{k}}T_{\mathbf{k}}\,{\rm Im}\,G(\mathbf{k},E). \tag{3}$$

In Eq. (3), $G(\mathbf{k},E)$ represents the quasiparticle Green function and its imaginary part is defined as

$${\rm Im}\,G(\mathbf{k},E)=u_k^2\frac{\Gamma}{(E-E_k)^2+\Gamma^2}+v_k^2\frac{\Gamma}{(E+E_k)^2+\Gamma^2}, \tag{4}$$

where u_k and v_k are the usual superconducting coherence factors and Γ is the quasiparticle damping rate. $E_k=\sqrt{[\xi_k^2+\Delta_k(T)^2]}$ represents the quasiparticle energy and ξ_k is obtained from the tight binding band structure defined as $\xi_k=-2t[\cos(k_x)+\cos(k_y)]-\mu$ where μ is the chemical potential. Qualitatively similar results would be obtained with the $t-t'$ band structure more appropriate for Bi2212.

The superconducting order parameters $\Delta_k(T)$ investigated in the present calculation are $d_{x^2-y^2}$ symmetry, extended $s+d_{x^2-y^2}$, and $s+id_{x^2-y^2}$. The d-wave superconducting order-parameter symmetry is given by

$$\Delta_{\mathbf{k}}^d(T)=\frac{\Delta(T)}{2}[\cos(k_x)-\cos(k_y)] \tag{5}$$

and the extended s-wave symmetry is given by

$$\Delta_{\mathbf{k}}^s(T)=\frac{\Delta(T)}{2}[\cos(k_x)+\cos(k_y)], \tag{6}$$

where the temperature-dependent prefactor $\Delta(T)$ used for both the extended s-wave and $d_{x^2-y^2}$ symmetries is

$$\Delta(T)=\Delta_0\tanh[1.76\sqrt{(T_c/T-1)}]. \tag{7}$$

In the present work, the same form of tunneling matrix element $T_{\mathbf{k}}$ is assumed for both elastic and inelastic tunneling, and is given by

$$T_{\mathbf{k}}=T_0|\mathbf{v}_g\cdot\mathbf{n}|\exp\left(\frac{-k^2+(\mathbf{k}\cdot\mathbf{n})^2}{(\mathbf{k}\cdot\mathbf{n})^2\theta_0^2}\right), \tag{8}$$

where $\mathbf{n}$ is the normal vector to the tunneling interface and $\mathbf{v}_g=\nabla\xi_k$ is the normal-state quasiparticle group velocity. θ_0 determines the width in $\mathbf{k}$ space of the line of states selected by $T_{\mathbf{k}}$.The matrix element of Eq. (8) is a modification of that proposed in Ref. 24 in that it incorporates the effect of the quasiparticle group velocity. The group velocity factor was first discussed for tunneling in Ref. 25. It is particularly important to include this factor in the case of HTSC due to the presence of the van Hove singularity (VHS) in the band-structure density of states which, however, does not appear in the experimentally measured tunneling density of states. The prefactor T_0 can be adjusted to vary the relative contributions of the elastic and inelastic tunneling channels to the total current across the tunnel junction. In the calculations presented in this paper, $T_0^{\rm inelastic}=\sqrt{(\pi)}T_0^{\rm elastic}$.

The spin-fluctuation-mediated inelastic channel is determined by the spectral width of AFMSF's, denoted by $D(E)$,

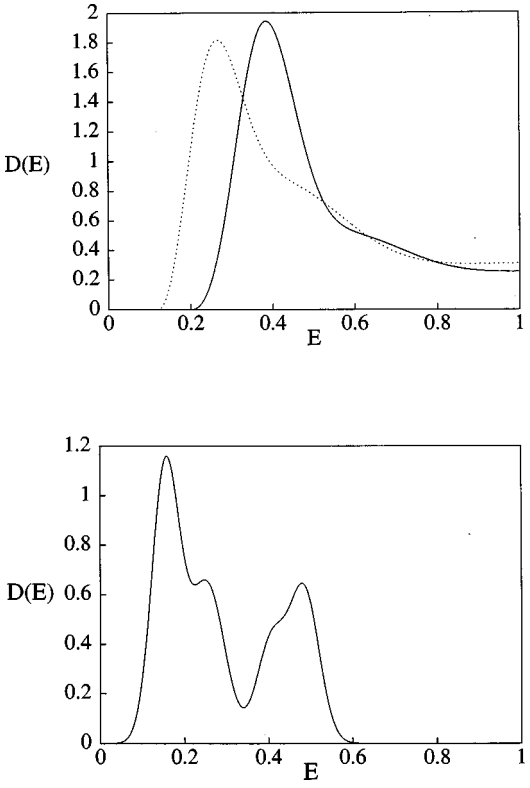

FIG. 1. The spin-fluctuation spectral function, $D(E)$, (upper panel) and the phonon spectral weight (lower panel) used in Eq. (2) for inelastic quasiparticle tunneling. $D(E)$ is calculated for $T/T_c = 0.8$ (dotted line) and $T/T_c = 0.01$ (solid line).

in Eq. (2). The dependence of $D(E)$ on temperature and energy E has been studied[12] before where $D(E)$ was calculated from

$$D(E) = \sum_{\mathbf{q}} (g/t)^2 \, \mathrm{Im}\, \chi(\mathbf{q},E). \tag{9}$$

In Eq. (9), g/t represents a coupling constant and $\chi(\mathbf{q},E)$ was calculated using a random-phase approximation formalism.[12] One of the results of that work[12] is that the onset of superconductivity at T_c results in a shifting of spectral width in $D(E)$ to energies above $E = 2\Delta(T)$. In the present work, the model for $D(E)$ which captures the essential features of the calculations of Ref. 12, is shown in the top panel of Fig. 1 for two temperatures ($T/T_c = 0.8$ for the dotted line and $T/T_c = 0.01$ for the solid line). The shifting of the peak in $D(E)$ to $E \geqslant 2\Delta(T)$ for $T/T_c = 0.01$ reflects the development of the sin gap due to superconducting feedback effects.[12] The position of the peak in $D(E)$ is chosen to be at $2\Delta(T)$.

The lower panel of Fig. 1 depicts the phonon spectral weight from Ref. 21. This is used to estimate the possible contribution of phonon-mediated inelastic tunneling processes using Eq. (2) above.

III. NUMERICAL RESULTS

Results for elastic an inelastic SIS tunneling are shown in Figs. 2–8. Figures 2, 3, 4, and 5 are calculated with $\mu = -0.2t$ in the tight-binding band structure $\xi_k = -2t[\cos(k_x) + \cos(k_y)] - \mu$ and illustrate a variety of SIS dI/dV curves for $d_{x^2-y^2}$, extended $s + d_{x^2-y^2}$, and extended $s + id_{x^2-y^2}$ order parameters. In Fig. 2 for $T/T_c = 0.01$ and Fig. 3 for $T/T_c = 0.8$, the right-hand column of the three figures illustrates the case where the tunneling is directional with $\mathbf{n}$ along the k_x axis and $\theta_0 = 0.1$ rad in Eq. (8) and the left-hand column is for the case of no directional tunneling where $T_{\mathbf{k}} = 1$. The group velocity factor $|\mathbf{v}_g \cdot \mathbf{n}_k|$ is also set to unity in calculating the results of Figs. 2 and 3 because a value of $\mu = -2.0t$ results in a Fermi surface over which the magnitude of the quasiparticle group velocity is relatively constant.

A number of interesting features are evident in Figs. 2 and 3. The choice of $\mu = -2.0t$ places the intersection of the Fermi surface at $k_x = \pi/2$ and results in the peak positions in the dI/dV curves being located at approximately half of $2\Delta_{\max}$ where $\Delta_{\max}$ is the maximum value in the BZ of either of the three order-parameter symmetries, $d_{x^2-y^2}$, extended $s + d_{x^2-y^2}$, and extended $s + id_{x^2-y^2}$, investigated in this work. The $s + d_{x^2-y^2}$ case is particularly interesting as shown in the second panel on the right-hand column of Fig. 2 where the directional matrix tunneling element of Eq. (8) is used in calculating dI/dV. The extended $s + d_{x^2-y^2}$ gap is close to zero for those states along the selected k_x axis which intersect the Fermi surface in this figure and this results in there being very little evidence of a superconducting gap in the directional tunneling conductance. The result of angle averaging the same gap symmetry over more k states as depicted in the second panel on the left-hand side of Fig. 2 (where $T_{\mathbf{k}} = 1$) incorporates additional portions of the Fermi surface in which the extended $s + d_{x^2-y^2}$ is nonzero.

It can also be seen in the right-hand columns of figures in both Figs. 2 and 3 that directional tunneling enhances the ratio of the peak height to high bias voltage conductance and tends to yield dI/dV curves that resemble some of the experimental curves more closely.[1,2] Furthermore, the combined effect of the elastic tunneling channel and the spin-fluctuation and phonon-mediated inelastic channels (the contributions for the latter are depicted in the lower section of each of the panels of Figs. 2 and 3) results in a broad dip feature in the dI/dV curves. The position of the dip features in the figures of the current work are not at exactly three times the gap, where the gap is taken as approximately half of the value of the position of the main SIS dI/dV peak in the figure. In the present work, the exact location of the dip feature, which appears in the combined elastic and inelastic tunneling conductance, is determined by factors such as the degree of quasiparticle damping Γ in $G(\mathbf{k},E)$ (which governs the width of the main SIS conductance peak), the exact shape of the spectral weight $D(E)$ and the relative magnitudes of the contributions from phonon and spin-fluctuation-mediated inelastic tunneling channels, and the value chosen for the chemical potential (μ). The position of the dip feature in the present work lies between two and three times the gap but can be adjusted to be at three times the gap, as is seen experimentally,[5] by suitable choice of parameters in $G(\mathbf{k},E)$ and $D(E)$.

In Fig. 4, a comparison of the contributions of the spin-fluctuation-mediated inelastic tunneling channels is illustrated for the three gap symmetries, $d_{x^2-y^2}$, extended s

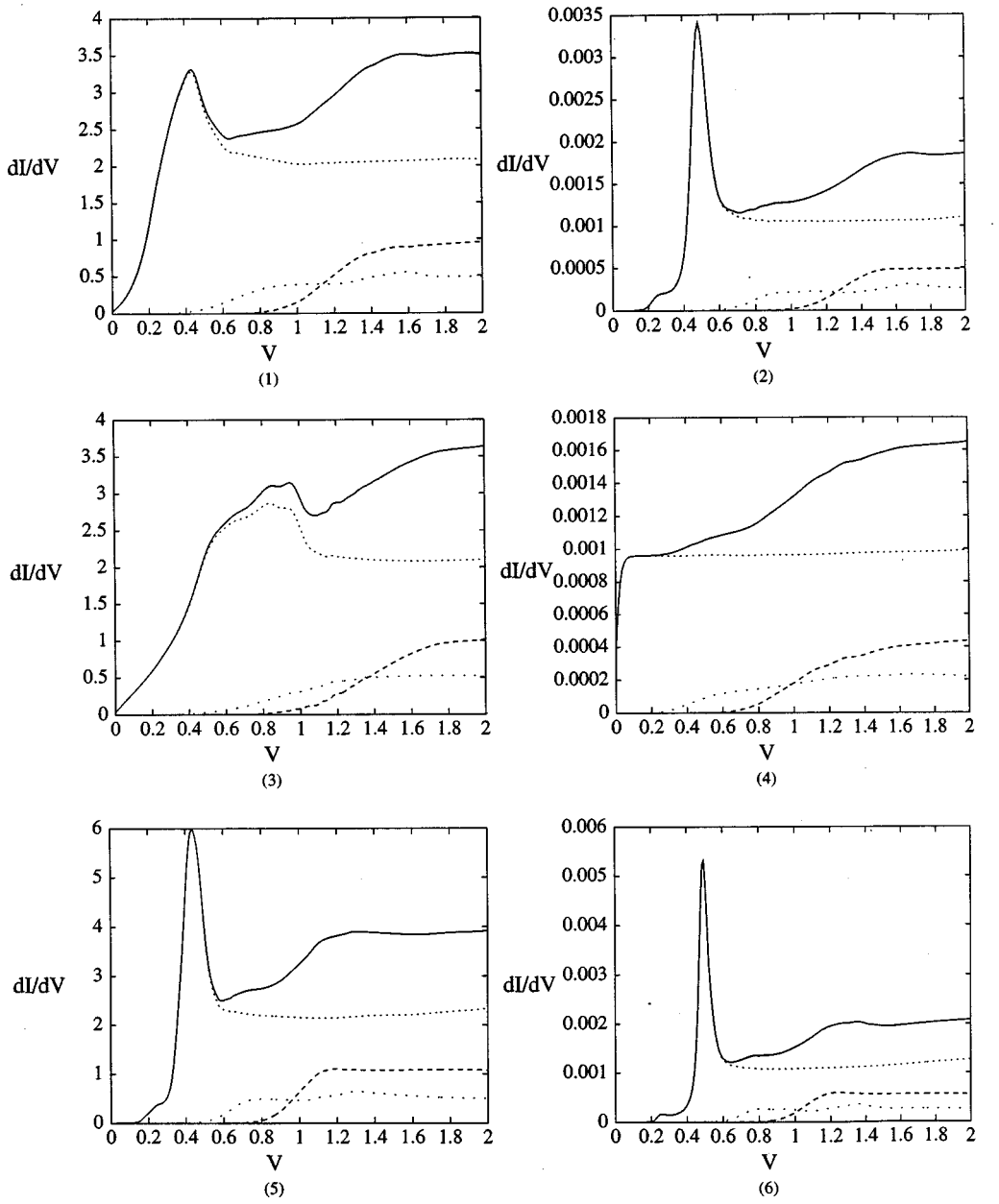

FIG. 2. SIS quasiparticle tunneling conductance curves (dI/dV) at a temperature $0.01T_c$ between two $d_{x^2-y^2}$ superconductors [panels (1) and (2)], two extended $s+d_{x^2-y^2}$ superconductors [panels (3) and (4)] and two extended $s+id_{x^2-y^2}$ superconductors [panels (5) and (6)]. The voltage is in units of $2\Delta_{\max}$ where $\Delta_{\max}$ is the maximum value in the BZ of the **k**-dependent order parameter being presented in any particular figure. The value of the chemical potential $\mu=-2.0t$ in all of the curves. The left-hand side of the figure is calculated without tunneling directionality and the right-hand side uses the tunneling matrix element of Eq. (8) with the group velocity prefactor set to unity. In each panel, the lower dashed curve represents spin-fluctuation-mediated inelastic tunneling and the lower dotted curve represents phonon-mediated inelastic tunneling. The solid line represents the combination of the inelastic and elastic tunneling channels. Other key parameters used in calculating these dI/dV curves are $\Delta_0=0.2t$ and $\Gamma=0.005t$. In the case of the directional tunneling curves, $\theta_0=0.1$ rad and **n** in Eq. (8) is along the k_x axis. The factor $4eT_0^2/t\hbar$ in Eqs. (1) and (2) is set equal to unity in computing these curves.

$+d_{x^2-y^2}$, and extended $s+id_{x^2-y^2}$. The exact location of the onset threshold plays an important role in determining the location of the dip feature in the total dI/dV curves presented in this work.

Finally, in Fig. 3 for $T/T_c=0.8$, the dI/dV curves develop a small peak close to zero-basis voltage. This is similar to what is observed in conventional *s*-wave SIS conductance calculations.[23]

Figure 5 illustrates the effect of increasing the quasiparticle damping rate Γ on the shape of the dI/dV curves for the case of directional tunneling. Increased damping, Γ, lowers the ratio of the peak height to the height of the dI/dV curve for energies greater than the position of the peak and also changes slightly the location and the shape of the dip feature.

Figures 6 illustrates the effect of the Van Hove singularity in the underlying normal-state band structure on the *I-V* curve for an SIS tunnel junction with a $d_{x^2-y^2}$ symmetry on both sides of the junction for the case $\mu=-0.01t$. The solid

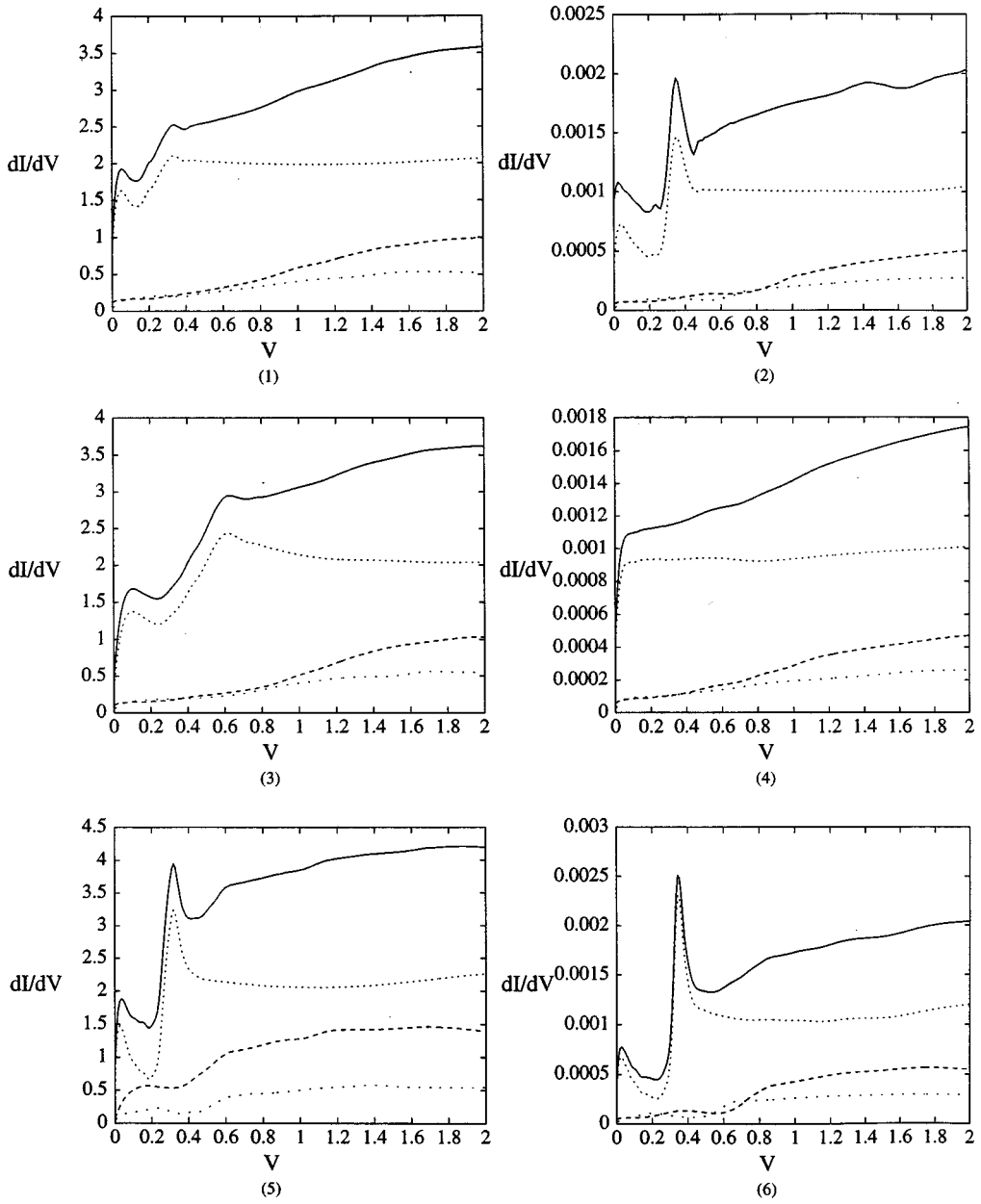

FIG. 3. The same as Fig. 2 except $T/T_c = 0.8$.

curves are calculations with the group velocity prefactor in the tunneling matrix element of Eq. (8) set to unity. The VHS in the underlying normal-state density of states results in a large peak in the *I-V* curve at the onset voltage threshold which now occurs at the maximum possible value of $0.4t$ because, in the case $\mu = -0.01t$, the Fermi surface is close to the $(k_x, k_y) = (\pi, 0)$ point. The effect on the *I-V* curve of incorporating the group velocity dependence of $T_{\mathbf{k}}$ of Eq. (8) is shown in the dotted curve in Fig. 6 where the prominent peak associated with the VHS is now significantly reduced. The inset of Fig. 6 shows the *I-V* curve for $\mu = -0.5t$ with the group velocity factor set to unity and illustrates how the VHS related peak shifts to a voltage above the onset in the *I-V* curve.

The conductance curves (dI/dV) for two *I-V* curves for $\mu = -0.01t$ are depicted in Fig. 7, including the effect of the inelastic tunneling channels. In the top panel of Fig. 7, which is generated from the dotted *I-V* curve of Fig. 6, a negative dI/dV results from the negative slope on the high voltage side of the peak in the corresponding dotted *I-V* curve of Fig. 6. The combination of the elastic and inelastic tunneling channels results in a dip feature above the main peak in the dI/dV curve. The difference in the dI/dV curves in the upper and lower panels of Fig. 7 is due to the choice of a different damping parameter Γ ($\Gamma = 0.005t$ in the upper panel and $\Gamma = 0.02t$ in the lower panel). The inset of the lower panel of Fig. 7 illustrates the dI/dV curve resulting from the combination of elastic tunneling and spin-fluctuation-mediated inelastic tunneling alone. The inset in the top panel illustrates the inelastic tunneling dI/dV separately for the total dI/dV curve of the top panel of Fig. 7, indicating the structure of the spin-fluctuation and phonon spectral weight functions that were shown in Fig. 1.

In recent PCT and STM measurements[2] on optimally and

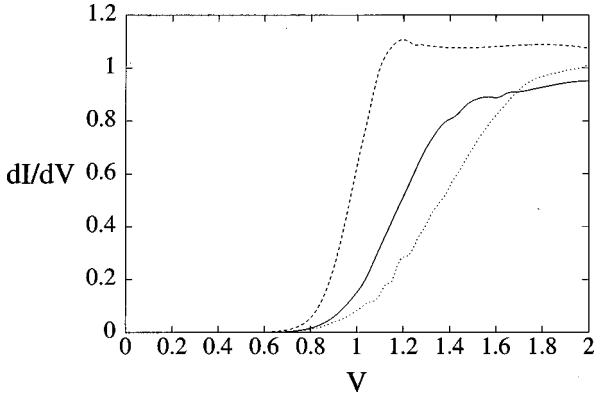

FIG. 4. A comparison of the spin-fluctuation-mediated inelastic tunneling channel contribution to the SIS dI/dV in the absence of tunneling directionality shown in the left-hand column of Fig. 2. The solid curve is the $d_{x^2-y^2}$ symmetry case, the dotted curve is the extended $s+d_{x^2-y^2}$ symmetry case, and the dashed curve is extended $s+id_{x^2-y^2}$ case. These curves are already shown in Fig. 2 and are reproduced here to show more clearly the onset of the inelastic tunneling channel for the three superconducting gap symmetries.

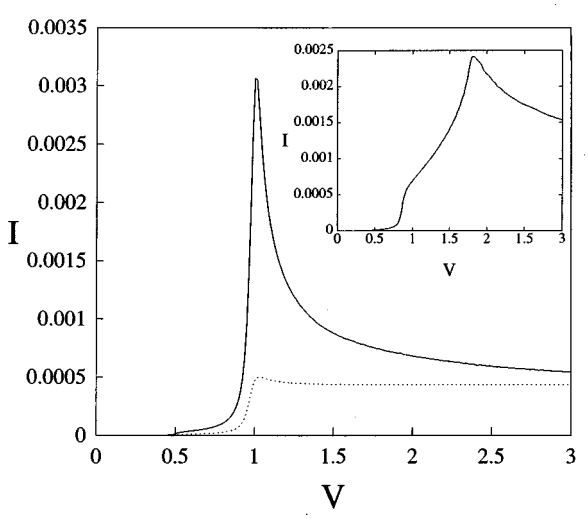

FIG. 6. Current-voltage curves (I-V curves) for quasiparticle elastic directional tunneling between two $d_{x^2-y^2}$ symmetry superconductors at $T/T_c=0.01$ and for $\mu=-0.01t$. The tunneling direction **n** is chosen to be along the k_x axis. The inset shows the case for $\mu=-0.5t$. The solid lines use Eq. (8) but with the quasiparticle group velocity factor set to unity. The dotted curve incorporates the full quasiparticle group velocity factor for the tight-binding band structure.

overdoped Bi2212, the voltage at which the SIS conductance peak is located decreases with increased hole doping. The dip feature maintains its position at close to three times the superconducting gap in the three samples in the experiment, but becomes shallower as the level of hole doping is increased. The level of hole doping (denoted by p in the companion paper of Ref. 1) is determined by using an empirical relation between the measured T_c and doping from Ref. 26. A comparison of the results of the present calculations for the tunneling conductance with the experimental results of Ref. 2 is shown in Fig. 8. In particular, curves A and C of Fig. 4 of Ref. 2 are depicted by the dotted curves of Fig. 8 in the upper and lower panels, respectively. The solid lines in Fig. 8 are the calculations.

In the present work, a more negative μ corresponds to overdoping and a change in μ from $-0.01t$ to $-2.0t$ produces a change in the Fermi surface from a nested surface ($\mu=-0.01t$) to one which intersects the k_x axis at (π/2,0) ($\mu=-2.0t$). This is the reason for the downward shift in the peak position in the theoretical curves shown in Fig. 8 which is determined by the value of $\Delta_k(T)$ on the relevant Fermi surface. In the top panel of Fig. 8, the solid theoretical curve and the dotted experimental curve have been lined up by choosing an appropriate value of the prefactor Δ_0 in Eq. (7). As can be seen from the lower panel of Fig. 8, by keeping the value for Δ_0 fixed, the downward shift of the peak in the theoretical curve matches quite closely that of the dotted experimental curve. This suggests that a significant contributing factor to the observed variation in the superconducting gap, with variations in doping, in Ref. 2 may originate in the change in the location of the Fermi surface in the Brillouin zone and not to a change in the strength of the superconducting pairing mechanism.

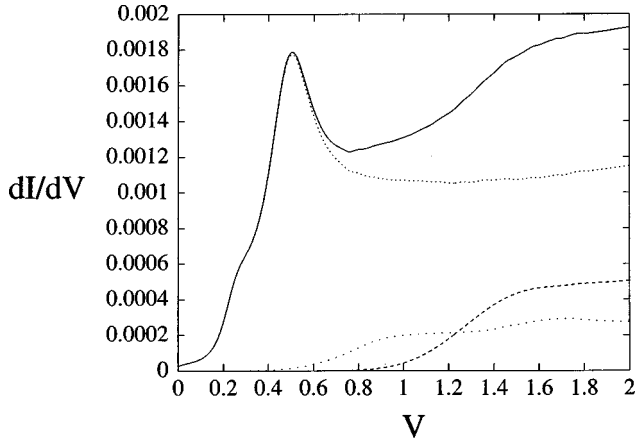

FIG. 5. The effect of increasing the quasiparticle damping rate Γ from $0.005t$ of panel (2) Fig. 2 to $0.02t$.

Furthermore, the observed variation in the shallowness of the dip feature with doping is also captured in the present work. In the calculations, the shallowness of the dip for $\mu=-2.0t$ is caused by an increase in the contribution of the elastic tunneling channel. For $\mu=-0.01t$, elastic tunneling results in a large peak at $2\Delta_{k=k_F}(T)$ but virtually no contribution for higher bias voltages. This is due to the fact that for directional tunneling along the k_x axis and, for $\mu=-0.01t$, the band structure results in an absence of states for elastic tunneling for voltages above $2\Delta_{k=k_F}(T)$. For more negative μ, i.e., $\mu=-2.0t$, the Fermi surface is located deeper in the Brillouin zone and this results in unoccupied states above the Fermi surface being available for tunneling at bias voltages greater than $2\Delta_{k=k_F}(T)$. The contribution to elastic tunneling from these states adds to the inelastic channel which starts from zero at approximately $2\Delta_{k=k_F}(T)$. The combined effect is a shallower dip feature than for the case $\mu=-0.01t$.

In the present work, we have not attempted to correlate

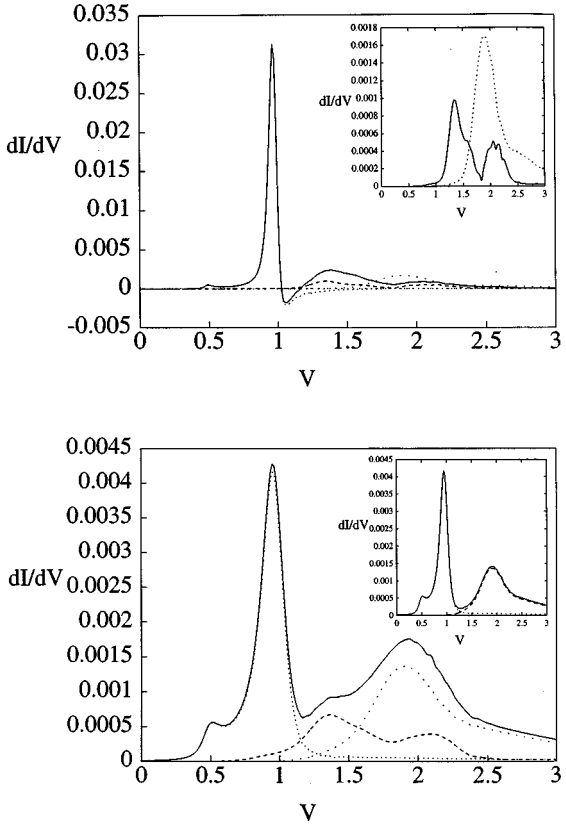

FIG. 7. The upper panel represents the dI/dV curve for the dotted curve of Fig. 6 with $\Gamma = 0.005t$ and the lower panel represents the dI/dV curve for the same conditions as the dotted I-V curve of Fig. 6, except that $\Gamma = 0.02t$. The inelastic spin-fluctuation-mediated and phonon-mediated channels are also included in these figures. The inset on the top panel shows the inelastic tunneling dI/dV alone, indicating how the shape is determined by the spectral weight curves of Fig. 1. The inset in the lower panel is a combination of the elastic and the spin-fluctuation-mediated inelastic channels alone. This combination produces a deep dip at approximately $2.5\Delta(T)$, similar to that seen in the experimental results of Refs. 1 and 2.

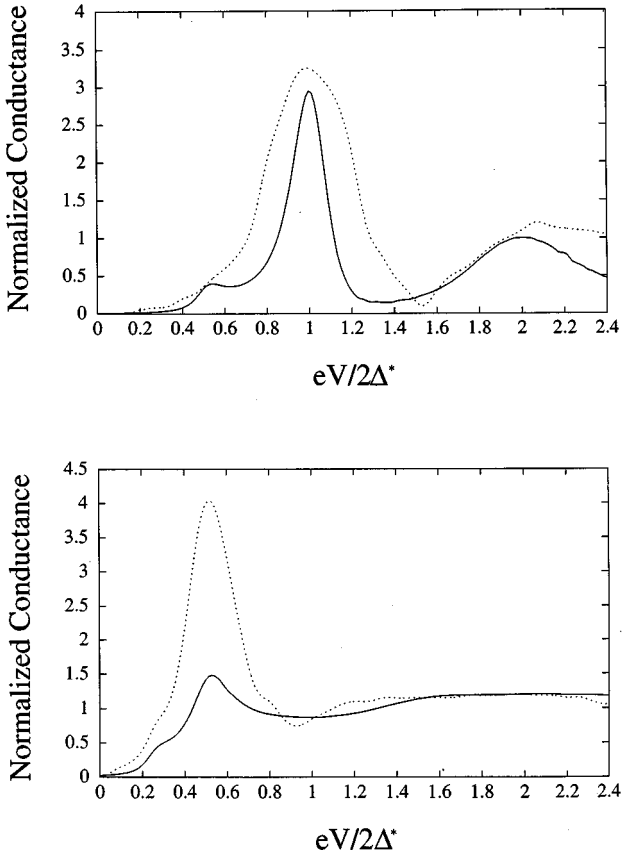

FIG. 8. A comparison between theoretical and experimental results for the quasiparticle tunneling in SIS junctions. In the upper panel, the dotted line depicts the experimental results for the optimally doped Bi2212 junction from curve A of Fig. 4 of Ref. 2. The solid line depicts the normalized theoretical calculation for $\mu = -0.01t$ and $\Gamma = 0.02t$. In the lower panel, the dotted line depicts the highly overdoped Bi2212 curve C of Fig. 4 of Ref. 2. The solid line depicts the normalized theoretical calculation for $\mu = -0.2t$ and $\Gamma = 0.02t$. Δ^* is defined by lining up the peak positions of the experimental and theoretical curves.

precisely the variation in chemical potential μ with a particular change in doping. In the experimental measurements of Ref. 2 the change in doping can be estimated to be approximately 50% (using Fig. 3 of Ref. 1) from curve A to curve C in Fig. 4 of Ref. 2. In any theoretical model, the dependence of μ on hole doping is determined by the details of the band structure and many-body interaction effects. For example, the shift in the main SIS conductance peak seen in Fig. 8 of the present work would occur for the $t-t'$ band structure:

$$\xi = -2t[\cos(k_x)+\cos(k_y)] - 4t' \cos(k_x)\cos(k_y) - \mu$$

with $t' = -0.45t$, for example, if the chemical potential μ was increased from a value $-1.75t$ (where the position of the chemical potential in the band coincides with that of the VHS) to $-2.0t$. This degree of change in μ would be reasonable for the doping variations investigated in Refs. 1 and 2.

While the variation in the position of the conductance peak and the evolution of the dip feature compare favorably with experiment, as can be seen in Fig. 8, the height of the conductance peak in the comparison with the experimental curve C in the lower panel of Fig. 8 is in disagreement. The noticeable narrowing of the experimentally measured conductance peak in going from curve A to curve C of Ref. 2 suggests that the quasiparticle damping rate (denoted by Γ in this work) is smaller in sample C compared to sample A of Ref. 2. In the theoretical curves in Fig. 8, Γ is held fixed at $0.02t$. A small decrease in Γ, which would be consistent with the experimental behavior, would yield a sharper, higher peak in the theoretical curve in the lower panel of Fig. 8 and enhance the agreement between the experimental curve C of Ref. 2 and the present calculations. The sensitivity of the tunneling conductance peak to variation in Γ can be gauged by examining Fig. 7 of the present work.

ACKNOWLEDGMENTS

We would like to acknowledge useful conversations with Chen-Hung Chang concerning the use of the Monte Carlo integration technique used in calculating the current-voltage curves in this paper. We would also like to acknowledge conversations with Professor J. F. Zasadzinski concerning his experimental data.

[1] N. Miyakawa *et al.*, Phys. Rev. Lett. **80**, 157 (1998).
[2] Y. DeWilde *et al.*, Phys. Rev. Lett. **80**, 153 (1998).
[3] Y. M. Nie and L. Coffey, Phys. Rev. B **57**, 3116 (1998); The calculations presented in Ref. 3 were carried out using definitions of the $d_{x^2-y^2}$ and extended *s*-wave gaps which did not include the conventional factor of one half (0.5) as indicated by Eqs. (1) and (11) of the text of Ref. 3. The numerical results in the figures of Ref. 3 are correct when this correction is taken into account. Furthermore, the absolute values for $I_{J1}(V,T)$, $I_{J2}(V,T)$, and $I_c(T)$ quoted in the test and figure captions of Ref. 3 and also shown in Figs. 1 and 2 should be divided by $1/2\pi$. Finally, the prefactor T_0 in Eq. (1) of Ref. 3 for the elastic and inelastic current contributions are related by $T_0^{\text{inelastic}} = \sqrt{(\pi)} T_0^{\text{elastic}}$. The discussions and conclusions in the text of Ref. 3 remain unchanged.
[4] J. F. Zasadzinski *et al.*, in *Spectroscopic Studies of High T_c Cuprates,* edited by I. Bozovic and D. van der Marel (SPIE, Bellingham, 1996).
[5] D. Coffey, J. Phys. Chem. Solids **54**, 1369 (1993).
[6] D. J. Harlingen, Rev. Mod. Phys. **67**, 515 (1995).
[7] C. C. Tsuei *et al.*, Science **271**, 329 (1996).
[8] K. Kouznetsov *et al.*, Phys. Rev. Lett. **79**, 3050 (1997).
[9] D. Coffey and L. Coffey, Phys. Rev. Lett. **70**, 1529 (1993).
[10] L. Coffey and D. Coffey, Phys. Rev. B **48**, 4184 (1993).
[11] K. Kouznetsov and L. Coffey, Phys. Rev. B **54**, 3617 (1996).
[12] L. Coffey, D. Lacy, K. Kouznetsov, and A. Erner, Phys. Rev. B **56**, 5590 (1997).
[13] C. Renner and O. Fischer, Phys. Rev. B **51**, 9208 (1995).
[14] Z. X. Shen *et al.*, Phys. Rev. Lett. **70**, 1553 (1993).
[15] D. J. Scalapino, Phys. Rep. **250**, 239 (1995).
[16] Y. Tanaka and S. Kashiwaya, Phys. Rev. Lett. **74**, 3451 (1995).
[17] Y. Tanaka and S. Kashiwaya, Phys. Rev. B **53**, R11 957 (1996).
[18] Y. S. Barash, A. A. Svidzinsky, and H. Burkhardt, Phys. Rev. B **55**, 15 282 (1997).
[19] J. X. Zhu and C. S. Ting, Phys. Rev. B **57**, 3038 (1998).
[20] M. Fogelstrom *et al.*, Phys. Rev. Lett. **79**, 281 (1997).
[21] G. A. Ummarino and R. S. Gonneli, Phys. Rev. B **56**, R14 279 (1997).
[22] C. B. Duke, in *Solid State Physics Advances in Research and Applications,* Suppl. 10 (Academic, New York, 1969).
[23] A. Barone and G. Paterno, *The Physics and Applications of the Josephson Effect* (Wiley, New York, 1982).
[24] M. Ledvij and R. Klemm, Phys. Rev. B **51**, 3269 (1995).
[25] J. Bardeen, Phys. Rev. Lett. **6**, 57 (1961); W. Harrison, Phys. Rev. **123**, 85 (1961).
[26] J. L. Tallong *et al.*, Phys. Rev. Lett. **75**, 4114 (1995).